The Journal of Supercritical Fluids 231 (2026) 106888

Contents lists available at ScienceDirect

The Journal of Supercritical Fluids

journal homepage: www.elsevier.com/locate/supflu

Continuous drying of alginate aerogel particles: Residence time measurement and process optimization under high pressure conditions

Erik Manke [a,*], Bennet Rastar [a], Alberto Bueno [b], Baldur Schroeter [a], Irina Smirnova [a,1]

[a] Institute for Thermal Separation Processes, Hamburg University of Technology, Eißendorfer Straße 38, Hamburg 21073, Germany
[b] aerogel-it GmbH, Albert-Einstein-Str. 1, Osnabrück 49076, Germany

HIGHLIGHTS

- Continuous $scCO_2$ drying of freely settling aerogel beads in a countercurrent column.
- Non-invasive optical residence time distribution measurement *in situ* under high-pressure operation.
- Statistical model links P, T, CO_2 and suspension flow to residence time and drying efficiency.
- ~400 µm alginate beads dried to residual ethanol level of 0.0053–0.0341 g/g.
- Aerogel quality preserved: 363 m^2/g surface area and 3.2 cm^3 /g pore volume.

GRAPHICAL ABSTRACT

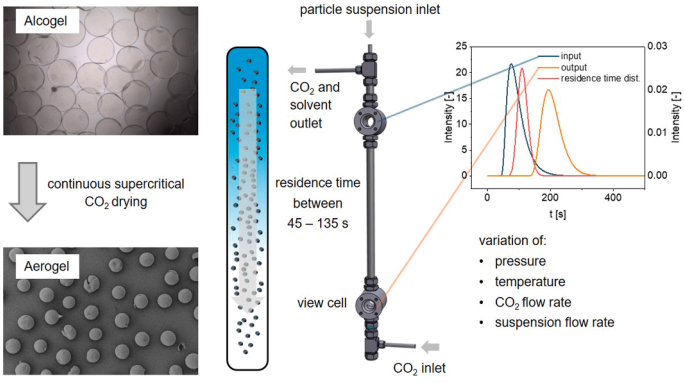

ARTICLE INFO

Keywords:
ScCO2 Aerogel drying
Continuous process
Optical RTD measurement
Countercurrent column

ABSTRACT

This study advances continuous supercritical carbon dioxide ($scCO_2$) drying of aerogel particles by introducing a non-invasive optical method to determine particle residence time in a countercurrent extraction column. In countercurrent operation, $scCO_2$ flows upward while the particle suspension in ethanol enters from the top. The method enables precise, real-time residence time measurement under high pressure conditions without disturbing the process. The effects of pressure (100–150 bar), temperature (40–80 °C), CO_2 flow rate (30–80 g/min), and suspension flow rate (10–45 g/min) on residence time and drying efficiency were accordingly analyzed. Experiments were performed in a 1.25 m high extraction column, with an internal diameter of 20.5 mm, using highly spherical alginate beads with a diameter of ~ 400 µm as a model system. Evidence of effective solvent removal throughout the whole operation range was provided by determination of the residual ethanol content in the intact aerogel beads after the drying process (0.0053–0.0341 $g_{ethanol}/g_{aerogel}$). The dried products featured a specific surface area of 363 ± 27 m^2/g, a mesopore volume of 3.2 ± 0.7 cm^3 /g, consistent with the typical range of alginate aerogels. The combined insights provide a comprehensive picture of the countercurrent column's operational response and allow the definition of practical operating windows. Elevated temperature and high

* Correspondence to: Scientific Coworker, Technische Universität Hamburg, Institut für thermische Verfahrenstechnik, Hamburg, Germany.
E-mail addresses: erik.manke@tuhh.de (E. Manke), bennet.rastar@tuhh.de (B. Rastar), alberto.bueno@aerogel-it.de (A. Bueno), baldur.schroeter@tuhh.de (B. Schroeter), irina.smirnova@tuhh.de (I. Smirnova).
[1] 0000–0003-4503–4039

https://doi.org/10.1016/j.supflu.2026.106888
Received 13 October 2025; Received in revised form 3 January 2026; Accepted 6 January 2026
Available online 7 January 2026

pressure provide the most favorable trade-off between short residence time and minimized residual ethanol, maximizing the time-specific yield. Overall, the approach establishes a robust, transferable framework for optimizing continuous $scCO_2$ drying of aerogel particles and supports extension to other particle sizes and formulations.

List of symbols and abbreviations

Physical quantities

g	Gravitational accelerationm·s^{-2}
d_p	Particle diameterm
ρ_p	Particle densitykg·m^{-3}
ρ_f	Fluid densitykg·m^{-3}
ν	Kinematic viscositym^2·s^{-1}
u_p	Particle settling velocitym·s^{-1}
D	Mutual diffusion coefficient (ethanol–CO_2)m^2·s^{-1}
v_j	Partial molar volume of component jm^3 ·mol^{-1}
$C_i(r,t)$	Concentration of component i inside the particlemol·m^{-3}
ε	Porosity–
τ	Tortuosity–
V_{pore}	Pore volumecm^3 ·g^{-1}
d_{pore}	Average pore diameternm
S_{BET}	Specific surface area (BET)m^2·g^{-1}

Dimensionless numbers

Ar	Archimedes number–
Re	Reynolds number–
Sc	Schmidt number–
Sh	Sherwood number–
Sh_f	Sherwood number (forced convection)–
Sh_n	Sherwood number (natural convection)–
Pe	Peclet number–
Θ	Efficiency metric combining residence time and residual ethanol–
ζ	Ratio of residence time to minimal theoretical drying time–

RTD analysis and efficiency metric

$C_{in}(t)$	Inlet tracer signal–
$C_{out}(t)$	Outlet tracer signal–
E(t)	Residence Time Distribution (RTD)–
$\bar{t}$	Mean Residence time–
τ_{res}	Residence times
$\tau_{dry,min}$	Minimum required drying times

Drying and material properties

$X_{\_EtOH}$	Residual ethanol content in the aerogel (mass fraction)g/g
$m_{EtOH,res}$	Absolute residual ethanol massg

Process parameters

T	Temperature°C
p	Pressurebar
$\dot{m}_{CO2}$	CO_2 mass flow rateg·min^{-1}
$\dot{m}_{susp}$	Suspension mass flow rate (ethanol + particles)g·min^{-1}

Chemistry and materials

$scCO_2$	Supercritical carbon dioxide-
EtOH	Ethanol-
G/M	Guluronic to mannuronic acid ratio of alginate-
$CaCl_2$	Calcium chloride (gelling agent)-

1. Introduction

In current scientific and industrial research, there is an increasing emphasis on enhancing the environmental performance, resource efficiency, and overall sustainability of industrial processes [1–3]. Continuous processing methods are progressively replacing traditional batch processes across various industries to achieve these objectives. Although batch processes offer operational flexibility, they often encounter substantial limitations regarding scalability, energy efficiency, and resource management [4].

In contrast, continuous processes offer multiple advantages, including reduced capital investment, smaller plant footprints, enhanced safety, particularly for exothermic reactions and high-pressure conditions and improved mass and heat transfer, all of which contribute to greater overall efficiency. Continuous operations also allow higher automation levels, improved responsiveness to feedstock variability, and more consistent product quality [5–7]. This shift is particularly evident in industries historically reliant on batch processing, such as pharmaceuticals and biopharmaceuticals, where economic pressures necessitate reduced production costs and enhanced efficiency [4,6,8,9].

A particularly compelling application for continuous processing lies in the drying of wet particles to produce aerogels using $scCO_2$ [10–12]. Aerogels, characterized by their exceptional high porosity, lightweight structure, and large inner surface area, have immense application potential across diverse fields, including insulation [13], catalysis [14], pharmaceuticals [15], and aerospace engineering [16]. Despite their extraordinary attributes, aerogels remain limited in commercial adoption [16], largely due to the high costs and complexities associated with their manufacturing processes, particularly the drying stage, which is conventionally performed through batch $scCO_2$ drying. This drying step, typically executed in high-pressure autoclaves, is notably resource-intensive and expensive, representing a significant barrier to wider market acceptance compared to more economically viable insulation materials, such as polyurethane foam or expanded polystyrene [17].

The complete removal of ethanol during aerogel drying is essential, as residual ethanol can compromise the material's mesoporous structure and its resulting thermal and mechanical properties. However, extracting the final traces of ethanol in batch processes is inherently inefficient, demanding disproportionate amounts of energy and prolonged extraction times, further exacerbating production costs [18]. Consequently, life cycle analyses consistently highlight the drying phase, including the use of high-pressure equipment, as the primary contributor to both economic and environmental impacts in aerogel production [19,20].

Recent work underscores clear advantages of continuous $scCO_2$ drying over conventional batch methods for aerogel production. As early as 1953, Sargent and Davis [21] described a continuous flow-through route for silica aerogels in which a silica sol is conveyed through a heated high-pressure tube and dried above the critical conditions of the pore liquid, a hot let-down prevents rewetting at discharge. Drying thus occurs in transit under very high temperature (~425 °C) and pressure (≈ 250 bar), with associated drawbacks: high energy demand, stringent safety requirements, risk of thermal sintering, reliance on solvent systems compatible with such temperatures, and limited applicability beyond inorganic silica. In a more recent concept, Ruiz and Clavier [22],

implement a continuous line for granular silica aerogels using fluidized or moving beds in which $scCO_2$ serves simultaneously as the fluidizing gas and the drying medium, continuously percolating the bed to extract the pore solvent. While this ensures strong mass transfer, it entails high $scCO_2$ throughput. Steinhagen and Herber [23] adopt a countercurrent architecture in which wet gel bulk solids are conveyed by a screw through a fixed high-pressure vessel while $scCO_2$ flows countercurrently to remove solvent; this offers compactness and a tunable residence time (via screw speed) but introduces mechanical complexity, moving parts and seals in high-pressure service, susceptibility to wear/bridging, and potential shear on fragile wet gels. Complementing these engineered approaches, Mißfeldt et al. [24] demonstrated a countercurrent column in which individual wet-gel beads sediment freely against an upward $scCO_2$ stream. In this configuration, residence time is governed directly by operating conditions (pressure, temperature, and flow rates) through their effect on buoyancy and drag, rather than by mechanical conveyance or bed hydrodynamics. By avoiding fixed-bed operation, the concept circumvents bed-scale maldistribution and convective complications, enabling faster solvent removal for discrete particles. Collectively, these approaches delineate the state of the art and reinforce that continuous $scCO_2$ drying is a promising pathway to reduce production costs and improve scalability, thereby addressing key barriers to broader commercial adoption of aerogels [24].

Effective characterization and optimization of these continuous processes depend on accurately quantifying and controlling the particle residence time in the drying system. The residence time distribution (RTD) analysis is a critical tool for identifying phenomena such as dispersion, backmixing, and bypass flows, thereby directly guiding process design and operational strategies to improve performance [25,26]. However, measuring RTD under high-pressure conditions presents notable challenges due to complex particle interactions, variable particle properties, and demanding operational conditions [27,28].

To tackle these challenges, we employed an optical technique using dayglow color pigments as tracers incorporated directly into the aerogel particle matrix. Real-time fluorescence measurements captured through optical techniques provide precise and instantaneous RTD data, allowing comprehensive analysis without interrupting operations or altering process conditions. Optical methods offer inherent advantages, including safety, non-invasiveness, and real-time monitoring capabilities, significantly surpassing the limitations of conventional chemical or radiometric tracer methods [28].

Based on this method, we investigated how key operating parameters such as pressure, temperature, CO_2 flow rate, and the flow rate of the particle suspension in ethanol influenced particle residence time and drying efficiency in a continuous $scCO_2$ drying column. Our aim was to quantify the effects and interactions of these parameters, establish a statistical description linking operating settings to residence time and drying outcomes (e.g., residual ethanol), and delineate practical operating windows for stable, efficient operation. Ultimately, this provides guidance that can be transferred to other particle systems and sizes.

2. Materials and methods

2.1. Materials

Carbon dioxide (≥99.9 %) was purchased from Linde AG, Pullach, Germany. Anhydrous ethanol (99.9 %) and calcium chloride dihydrate (≥ 98 %) were obtained from Carl Roth GmbH & CO.KF, Karlsruhe, Germany. The sodium alginate used in this study was kindly provided by IFF Nutrition & Health Germany GmbH & Co KG, Walsrode - Bomlitz (IFF Division Pharma Solutions), Germany. The alginate had a guluronic-to-mannuronic acid ratio (G/M) of 0.57 and a weight-average molar mass of 280 kDa. Fluorescent dayglow pigment "Tages-Leucht-Farbe Goldorange" (Kremer Pigmente GmbH & Co. KG, Aichstetten, Germany) was used as optical tracer. The pigment is a polymer-bound fluorescent dye mixture containing talc (1–5 %), organic xanthen-based dye components (<0.5 %), and trace amounts of stabilisers (<1 %). The powder is water-insoluble and has an average particle size of approx. 5 μm. All chemicals were used without further purification, and deionized water from the Hamburg University of Technology utility system was used throughout the study.

2.2. Particle preparation

The gel particles were prepared according to previous works using a continuous JetCutter technique [29,30] (the used JetCutter parameters can be found in the Supplementary Material, table S1). A 0.5 wt% calcium chloride dihydrate solution served as the gelling bath. A 2 wt% sodium alginate solution prepared at room temperature was used as the precursor. For the tracer particles, 0.4 g of fluorescent pigment was added per liter of alginate solution (0.04 wt%), ensuring homogeneous distribution without altering the rheological properties of the polymer. After complete gelation, the beads were thoroughly washed with deionized water to remove excess calcium ions. Subsequently, solvent exchange was performed in repeated steps using 99.9 wt% anhydrous ethanol. After each exchange, the particles were allowed to equilibrate for 24 h. With each step, the internal solvent composition shifted gradually toward higher ethanol contents. The exchange procedure was repeated until the surrounding liquid phase reached at least 98 wt% ethanol, as determined with a density meter (Anton Paar DMA 4500 M, Graz, Austria).

2.3. $ScCO_2$ drying column and particle detection system

Drying of the alcogel particles was carried out in a continuous countercurrent $scCO_2$ drying column. The experimental setup builds on the continuous drying concept introduced by Mißfeldt et al. [24], in which initial experiments demonstrated the practical feasibility of such a process. In contrast to that earlier study, the present work provides a quantitative experimental validation of the underlying theoretical concepts, including particle residence-times, residual ethanol contents and the dependence on key process parameters.

The drying experiments were conducted in a 1.25 m high continuous $scCO_2$ column constructed from a high-pressure tube with an internal diameter of 20.5 mm. $ScCO_2$ entered the column at the bottom and exited at the top. Alginate alcogel particles suspended in ethanol were introduced at the top of the column. Due to their higher density in comparison to $scCO_2$, the particles sedimented downward against the upward flow of $scCO_2$. During their descent, ethanol was extracted from the pores of the gel matrix by the $scCO_2$. The extracted ethanol, along with the $scCO_2$, exited the system at the top (see Fig. 1).

To enable a quantitative, non-invasive determination of the particle residence time under these countercurrent high-pressure conditions, an optical tracer-based detection approach was implemented. Fluorescent color pigments which absorb blue and UV light while emitting photons in the yellow-orange spectrum were used as tracers. Due to their average size of 5 μm, the fluorescent pigments could be incorporated into the alginate matrix without affecting the physical properties of the polymer, particularly its density. For 1 L of alginate solution, 0.4 g of pigment was added. A blue LED from Osram, (LE B P1MR, Osram, Munich, Germany) was used to excite the pigments. A long-pass filter at 500 nm (long-pass filter OD 4, Edmunds, Mainz, Germany) was used, so that only the emitted color spectrum of the tracer was recorded and not the LED. All wavelengths shorter than 500 nm were filtered out by the long-pass filter and only light with a higher wavelength was allowed to pass through (see Fig. 2).

To ensure that the emitted photons of the tracer's pigments can be detected, two view cells made of sapphire glass were integrated into the high-pressure column, which can withstand pressures of up to 200 bar. An APS-C EXMOR® CMOS sensor from Sony (Sony Corporation,Tokio, Japan), served as the detector. The complete setup for detecting the tracer particles is shown in Fig. 3.

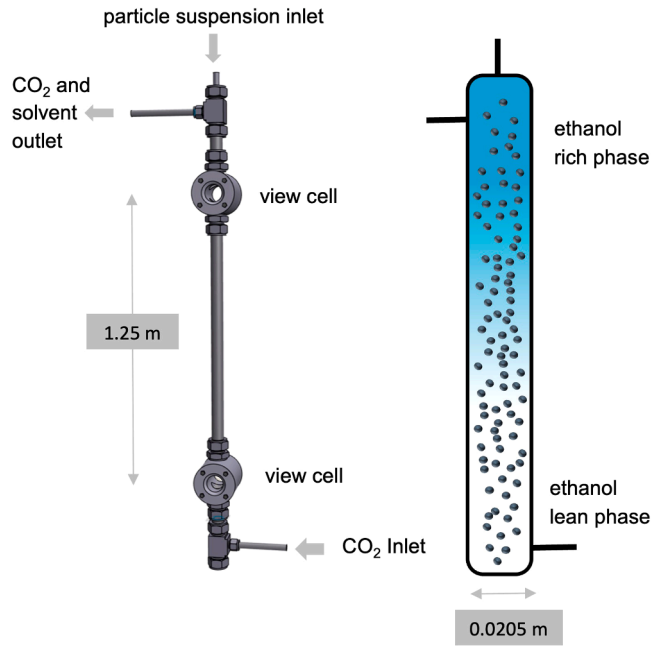

Fig. 1. schematic drawing of continuous countercurrent supercritical drying column (left) and visualization of ethanol rich and lean zones inside of the column (right).

The alcogel particles (alginate gels filled with ethanol) containing the tracer were added to the column as a pulse input. Since the addition of particles in a high-pressure process is particularly challenging, only a pulse input is suitable for measuring the residence time. Ideally, the tracer would be injected as a Dirac pulse at the column inlet, because an instantaneous input yields the RTD directly, reduces tracer demand, and accelerates a precise evaluation. In our setup, a true Dirac pulse could not be realized; instead, the tracer was injected as rapidly as practicable to approximate a short impulse, as commonly reported in the literature [31,32]. However, even the very short transfer section between the injection point and the column already caused substantial dispersion of the particle suspension. To ensure that we quantify dispersion originating from the column rather than from the feed line, a second sapphire viewing window was integrated at the top of the column. This configuration allowed us to record the effective inlet signal immediately upon entry into the column and in parallel, the outlet signal at the column bottom. Measuring both signals with identical sampling conditions enables normalization and subsequent convolution/deconvolution, so that the residence time distribution of the column was obtained, despite an imperfect pulse and the unavoidable pre-dispersion in the feed.

2.4. Supercritical drying procedure

Initially, the column was pressurized and heated to the desired setpoints using pure $scCO_2$. Once stable operating conditions were achieved (constant temperature, pressure, and flow rates), ethanol was introduced into the column to establish the ethanol-rich phase. After steady-state was reached, the particle suspension was fed into the system. Due to the shift in ethanol concentration caused by particle introduction, a second stabilization phase was required. Once steady-state conditions were re-established, tracer particles were added to initiate the residence time distribution (RTD) experiment. The experiment continued until no tracer particles were visible in the bottom sight glass. The particle feed was then stopped, and the ethanol feed was kept running only until any particles still present in the feed line or the upper section of the column had sedimented to the bottom and been collected. Afterwards, the system was purged with fresh $scCO_2$ until no further ethanol could be recovered downstream in the separator. Finally, the column was depressurized at a controlled rate of 2 bar/min, and the dried samples were collected. Table 1 summarises all operating ranges and particle characteristics used in the continuous drying experiments. The maximum

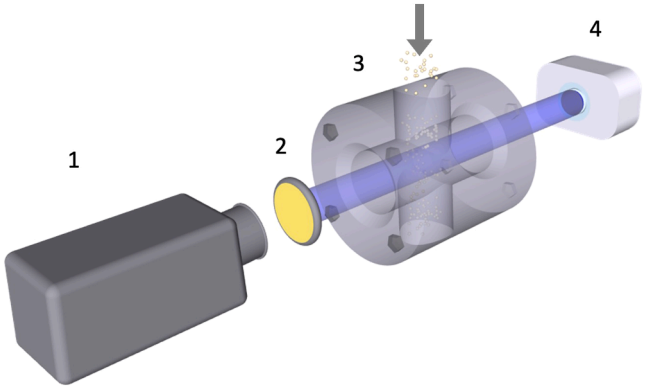

Fig. 3. Schematic drawing of particle detection system. 1) APS-C EXMOR® CMOS-Sensor from Sony, 2) 500 nm Longpassfilter OD 4 from Edmunds, 3) high-pressure view cell, 4) Blue Light LED LE B P1MR from Osram.

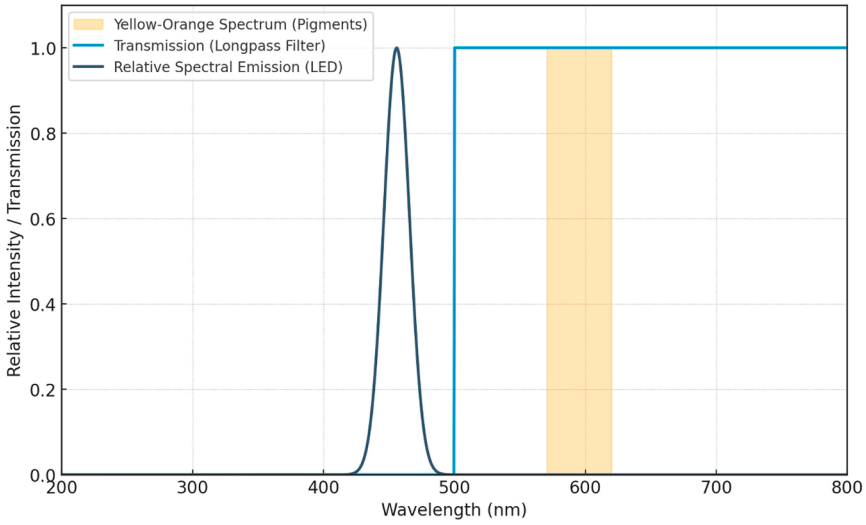

Fig. 2. Schematic representation of the LED light spectrum, the transmission profile of the longpass filter, and the emitted light of the tracer particles.

operating pressure of the experimental setup was limited to 150 bar; this technical constraint therefore defined the upper pressure level investigated in the present study. A complete overview of all experimental conditions and corresponding results for all experimental runs is provided in the Supplementary Material (Table S2)

2.5. Aerogel characterisation

Thermogravimetric analysis was used to determine the residual ethanol content. Approximately 100 mg of sample was used in each run. Thermogravimetric analysis was performed using a Linseis STA Series instrument (Linseis Messgeräte GmbH, Selb, Germany) The heating protocol included an isothermal step at 60 °C to quantify ethanol, followed by heating to 110 °C at 5 K/min to differentiate between ethanol and water. Specific surface area (BET) and pore size distribution (BJH) measurements were carried out using a Quantachrome NOVA 3000e analyzer after 12 h degassing at 60 °C under vacuum (Quantachrome Instruments, Boynton Beach, FL, USA). The particle residence time and resulting RTD functions E(t) were quantified following the ADE-based signal processing methods described in Section 2.6 (fitting, normalization, FFT convolution, inverse FFT).

2.6. Data processing

A key innovation of our method is that the tracer signal is quantified by explicitly counting individual fluorescent particles rather than integrating image intensity. For this purpose, the recorded image material was analyzed using a Python-based image-processing workflow. The particles were detected through a binary segmentation approach: the grayscale video frames were thresholded to produce black-and-white (binary) images, in which connected component analysis was applied to identify individual particle regions. Only regions exceeding a minimum area threshold were classified as valid particles, effectively filtering out noise and small artifacts. Tracking was performed using a frame-by-frame nearest-neighbor association, where particles are matched across consecutive frames based on minimal Euclidean distance within a defined search radius. By tracking the particles, both the trajectory and the speed of the individual particles can be determined and, especially for larger particles, it would also be possible to measure the particle size distribution. This also makes it possible to potentially analyze any shrinkage or swelling of the particles during the process.

To determine the residence time distribution (RTD) from experimental data, a structured signal-processing approach based on the advection-dispersion equation (ADE) was applied. This equation effectively describes the transport and dispersion of solutes in flow systems [33]. Experimental measurements yielded two time-resolved concentration signals: the inlet concentration $C_{in}(t)$ and the outlet concentration $C_{out}(t)$. Initially, both signals were individually fitted using an ADE to minimize experimental noise and obtain smooth representations suitable for subsequent analysis. The theoretical ADE for an open-open boundary condition in terms of the Peclet number (Pe) is described as follows [34]:

$$E(t) = \frac{1}{2}\sqrt{\frac{Pe}{\pi \bullet \theta}} \bullet \exp\left[-\frac{Pe \quad (1-\theta)^2}{4 \bullet \theta}\right] \tag{1}$$

Table 1
Range of process parameters evaluated in this study. Particle parameters were adopted from [24].

Process parameter	Range	Particle Properties	Average
Pressure [bar]	100 – 150	**D_{mean} [µm]**	421 ± 46
Temperature [°C]	40 – 80	**Porosity [-]**	0.94
CO_2 flow rate [g/min]	30 – 80	**Tortuosity [-]**	2.5
Suspension – flow rate [g/min]	10 – 45	**Skeletal density [kg/m³]**	1600

$$\theta = \frac{t}{\bar{t}} \tag{2}$$

Where $\bar{t}$ is the mean residence time. Following the fitting, both signals were normalized to ensure equal integrals (areas under the curves). This normalization is crucial, as it allows accurate convolution, which relates the inlet to the outlet signals through the system-specific RTD. The normalized RTD (E-function) can be expressed discretely as:

$$E(t) = \frac{C(t_i)}{\sum_i^{N_s} C(t_i)\Delta t_i} \tag{3}$$

The convolution integral relates the normalized inlet concentration $E_{in}(t)$ to the normalized outlet concentration $E_{out}(t)$:

$$E_{out}(t) = \int_0^t E_{in}(t') \bullet E(t-t') \bullet dt' \tag{4}$$

In this equation, *E(t)* acts as a weighting function, representing the fraction of solute exiting the system at time t, having entered at time t′.

2.7. Statistical analysis

Statistical analysis of the experimental data was performed using Design-Expert software (Version 22.0.6, Statcon, Germany). The experimental campaign was structured based on a Box–Behnken-type response surface design to investigate the influence of pressure, temperature, CO_2 flow rate, and suspension flow rate on process performance. The response variables considered were the mean particle residence time and the residual ethanol content of the dried aerogels. Due to thermodynamic constraints, not all factor combinations of a classical Box–Behnken design were experimentally accessible, resulting in a constrained design space. In particular, combinations of low pressure and high temperature would shift the system out of the single-phase supercritical region and were therefore not feasible. Consequently, the Box–Behnken design was employed as a structured framework for parameter variation rather than as a full, unconstrained design. A representative operating condition located close to the practical center of the feasible design space was repeated three times to assess experimental reproducibility and estimate experimental variability. The replicated experiments exhibited a relative standard deviation of 5.1 % for the mean residence time and 27 % for the residual ethanol content. One-way analysis of variance (ANOVA) was applied to evaluate the statistical significance of the model terms, with a significance level of $p < 0.05$.

3. Theoretical background

As a result of the counter-current configuration, an ethanol-rich zone formed in the upper section of the column and an ethanol-lean zone at the bottom. Since ethanol has a higher density than $scCO_2$ under the applied conditions, an inverse density gradient was established, with higher density in the upper part and lower density in the lower part of the column. Maintaining this gradient was essential for efficient and complete drying. The density profile is influenced by four key process parameters: temperature, pressure, and the flow rates of both the incoming $scCO_2$ and the particle suspension. These parameters not only affect the solvent concentration and density profiles within the column but also, in combination with three critical particle parameters, the bulk density, porosity, and particle diameter, influence the residence time of the particles.

Three forces act on each particle during its descent through the column. The interplay of these forces determines the terminal velocity of the particles and, consequently, their residence time within the column.

Gravitational force: This force depends solely on the particle properties, such as density and volume.

$$F_G = m \bullet g = V_p \bullet \rho_p \bullet g \tag{5}$$

Where m is the particle mass, V_p is the particle volume, ρ_p is the particle density, and g is the gravitational acceleration.

Buoyancy force: This force opposes gravity and depends both on the particle diameter and on process conditions. Pressure and temperature influence the fluid density, while the flow rates determine the solvent concentration gradient along the column height.

$$F_A = V_P \bullet \rho_f \bullet g \tag{6}$$

Where ρ_f is the density of the surrounding fluid.

Drag force: This resistance force acts opposite to the direction of motion and is influenced by fluid viscosity and relative velocity. It is affected by all four process parameters as well as by the particle size and shape.

$$F_D = C_D \bullet \rho_f \bullet A \bullet u_p^2 \tag{7}$$

Where C_D is the drag coefficient, A is the projected particle cross-sectional area, and u is the relative velocity of the particle. The interaction of the three dominant forces acting on falling particles, gravitational, buoyant, and drag forces, can be described in a dimensionless form using the Archimedes number (Ar) and the Reynolds number (Re). The Archimedes number quantifies the ratio of gravitational driving forces to the viscous resistance of the surrounding fluid and is defined as:

$$Ar = \frac{g \bullet d_p^3 (\rho_p - \rho_f)}{\rho_f \bullet \nu^2} \tag{8}$$

Where ν is the kinematic viscosity of the fluid. Ar thus expresses the influence of density difference on particle settling relative to the fluid's viscous damping. The Reynolds number characterizes the ratio of inertial to viscous forces during the motion of the particle relative to the fluid and is given by:

$$\mathrm{Re} = \frac{u_p \bullet d_p}{\nu} \tag{9}$$

Together, the Archimedes and Reynolds numbers provide a dimensionless framework for describing particle motion in fluids. They form the basis for numerous empirical and semi-empirical correlations used to predict the terminal settling velocity and to classify the flow regime around the particle as laminar, transitional, or turbulent. Like the model proposed by Turton and Clark [35], which was also applied in the proof-of-concept study of the continuous drying column [24].

$$\mathrm{Re} = Ar^{1/3} \left[\frac{1}{\left(\frac{18}{Ar^{2/3}}\right)^{0.824} + \left(\frac{0.321}{Ar^{1/3}}\right)^{0.412}} \right]^{1.214} \tag{10}$$

This correlation provides a useful estimation of particle terminal velocity, but only under the simplifying assumption that the particles are completely dry and surrounded by pure $scCO_2$. In reality, this assumption introduces significant limitations. Under actual process conditions, the fluid density surrounding the particles changes continuously, due to both the ethanol concentration gradient and the falling motion of the particles through the drying column. Simultaneously, the density of the particles themselves changes over time as drying progresses. The drying rate of the particles is thus strongly influenced by the operating parameters of the process. The drying process can be described by a combination of two mass transport mechanisms: internal and external. Inside the particle, solvent removal proceeds as a superposition of diffusion and advection in the pore liquid. In addition to molecular diffusion, a convective contribution referred to as solvent spillage can occur. When $scCO_2$ enters the ethanol-filled pores, it mixes with the ethanol and forms a CO_2–ethanol solution with a larger specific volume than pure ethanol. Because the pore volume remains essentially constant, this expansion creates a temporary pressure increase inside the pores. The resulting pressure gradient drives a short pore-scale outward flow that pushes the CO_2–ethanol mixture from the interior toward the particle surface and into the surrounding fluid. [36]. The internal concentration field c(r,t) is then described by a spherically averaged advection–diffusion balance (superposition of diffusion and advection) [37].

$$\frac{\partial c_i}{\partial t} = \frac{\partial}{\partial r}\left(D\frac{\partial c_i}{\partial r}\right) + \frac{D}{r} \bullet \frac{\partial c_i}{\partial r} - \frac{1}{r}\frac{\partial}{\partial r}\left(c_i r \int_0^r \frac{D}{-v_j c_i}\left(\frac{\delta v_j}{\partial c_i}\right)\left(\frac{\partial c_i}{\partial r}\right)^2 dr\right) \tag{11}$$

Here, c_i denotes the concentration of component i in the pore liquid; t is time; r is the radial coordinate; D is the mutual (binary) diffusion coefficient of the ethanol–CO_2 mixture; v_j is the partial molar volume of compound j in the binary mixture. At the particle surface, ethanol is transferred into the surrounding $scCO_2$ phase. The external mass transfer coefficient is typically expressed in dimensionless form via the Sherwood number (Sh), which relates convective mass transfer to molecular diffusion. It depends on key dimensionless groups such as the Reynolds number (Re) and the Schmidt number (Sc), and includes contributions from both forced and natural convection. In mixed convection scenarios, such as the drying of aerogel particles in an upward $scCO_2$ flow, the Sherwood number can be decomposed into a forced component (Sh_f) and a natural component (Sh_n). The relative contribution of these mechanisms varies with particle size, while natural convection dominates for small particles due to low sedimentation velocities, forced convection becomes increasingly significant for larger particles. The overall Sherwood number, and thus the mass transfer coefficient, is also sensitive to process parameters such as temperature, pressure, and fluid composition. For instance, increasing the temperature generally enhances molecular diffusion and lowers fluid viscosity, thereby promoting both diffusion and convection. Crucially, pressure and temperature must be selected so that operation remains above the ethanol–CO_2 mixture's critical locus. Only under single-phase supercritical conditions are ethanol and CO_2 fully miscible, eliminating liquid–gas interfaces and associated capillary forces; this ensures uninterrupted extraction and maximizes the effectiveness of the combined diffusive–convective transport.

All process parameters that promote short drying times, such as elevated temperatures or reduced pressures, inevitably also affect the residence time of the particles in the column. This is due to the strong interdependence between drying kinetics and particle motion. A change in any operating condition alters not only the bulk fluid properties (e.g., density and viscosity) but also the mass transfer rate, which in turn influences the drying rate and therefore the particle density. This strong coupling makes it challenging to predict residence times or drying durations accurately using purely theoretical or steady-state models. It therefore becomes essential to support process design with experimental data, particularly under dynamic, real-process conditions where simultaneous changes in mass transfer, particle density, and fluid properties must be captured realistically.

4. Results and discussion

In this study, the influence of the critical process parameters, pressure, temperature, CO_2 flow rate, and the suspension flow rate, on the continuous $scCO_2$-drying of alginate alcogels was systematically investigated. For each experiment, the particle residence time within the drying column was measured using the specially designed experimental setup. The drying efficiency was assessed by the residual volatile content (ethanol + water; determined by TGA), with the residual ethanol content used for the evaluation. Subsequently, the physical properties of the dried particles were thoroughly characterized.

4.1. Influence of process parameters on residence time distribution

The process parameters for pressure and temperature were selected within ranges typically used for batch drying processes [10,18]. CO_2 and suspension flow rates were selected based on column dimensions and practical operational considerations, ensuring that the CO_2 flow rate was not excessively high to maintain an efficient drying process. To systematically evaluate the influence of all four process parameters, a structured multivariate experimental approach was employed, and the resulting data were analyzed using statistical modeling. The outcomes of this analysis are presented in Fig. 4.

It is clearly evident that temperature and pressure exert the most significant influence on the mean residence time, as particle settling velocity strongly depends on the fluid density (Fig. 4(a)). The data indicate an almost proportional relationship between mean residence time and fluid density. Particularly at low pressures and temperatures, even minor changes in pressure or temperature lead to substantial variations in density and consequently in residence time. At pressures around 150 bar, however, the increase in fluid density becomes very small due to the asymptotic compressibility of $scCO_2$. As a result, a further increase in fluid density with pressure would be expected to lead to a rise in mean residence time, but only to a very limited extent. In this regime, the incremental gain in residence time no longer justifies the additional energy required to compress the CO_2–ethanol mixture to higher pressures. The quality of the statistical model for the mean residence time was assessed using the ANOVA results (Table S3) and predicted versus actual plots (Figure S1(a)), provided in the Supplementary Material.

In Fig. 4(b), it can be observed that the CO_2 flow rate has only a minor influence on the mean residence time of the particles. Changes in residence time closely correspond to variations in the superficial velocity of the flowing $scCO_2$, directly affecting the net settling velocity of the particles. From this observation, it can also be concluded that the relatively low suspension feed rate does not lead to the formation of a pronounced ethanol concentration gradient within the drying column. If such a gradient were present, an increase in CO_2 flow rate would significantly alter the concentration profile along the column height. Consequently, this would result in a nonlinear relationship between CO_2 flow and particle residence time. This conclusion is further supported by Fig. 4(c), where it is demonstrated that varying the suspension flow within the investigated range has a negligible influence on the mean residence time of the particles. The slight increase can be attributed to the minor elevation in bulk fluid density resulting from the higher ethanol addition, which slightly extends the particle residence time. If an increase in suspension flow significantly altered the ethanol concentration profile within the column, a corresponding substantial

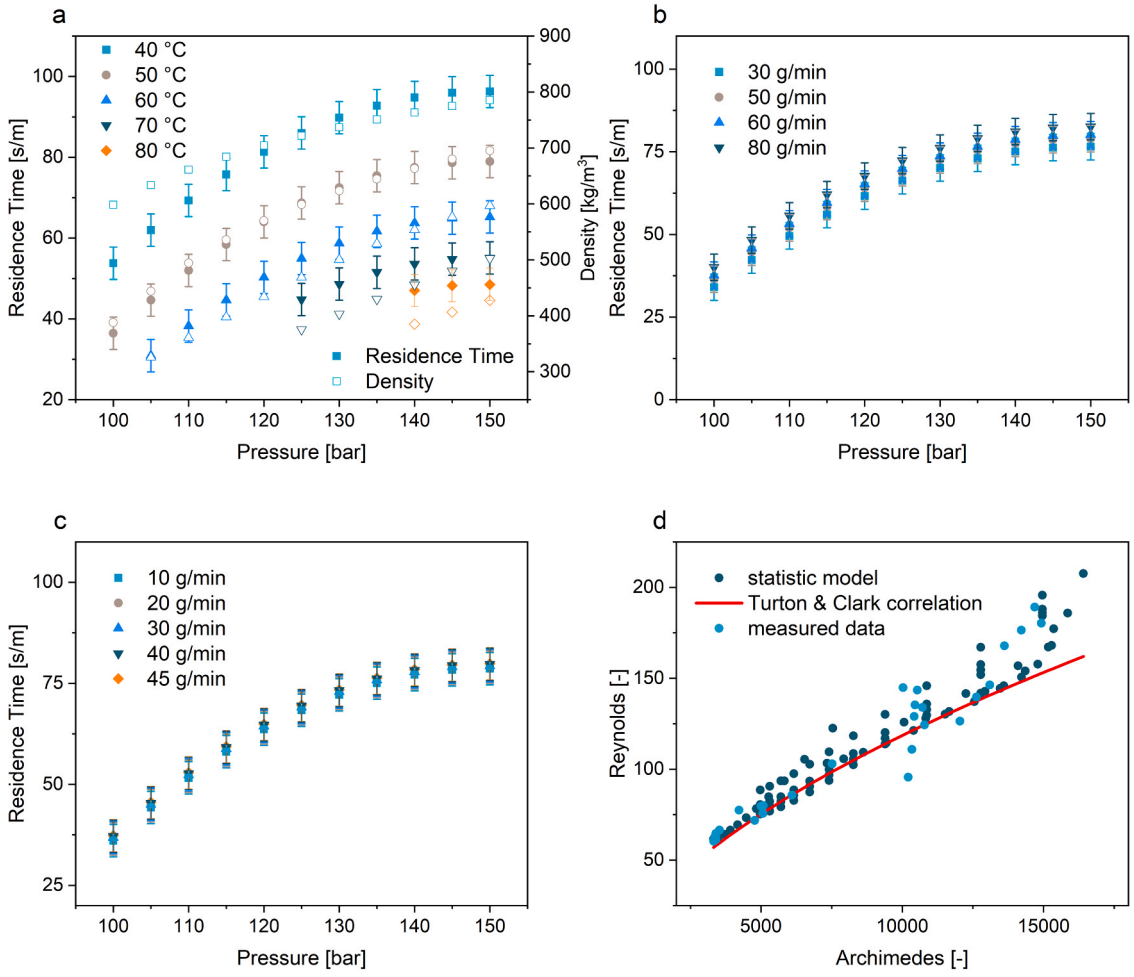

Fig. 4. Influence of process parameters on mean residence time: a) Influence of temperature and pressure at constant CO_2 flow rate (50 g/min) and constant suspension flow rate (20 g/min) on mean residence time (solid points) and their influence on the density of pure $scCO_2$ (open points). b) Influence of the CO_2 flow rate on mean residence time at constant temperature (50 °C) and constant suspension flow rate (20 g/min). c) Influence of suspension flow rate on mean residence time at constant temperature (50 °C) and constant CO_2 flow rate (20 g/min). d) Comparison between the purely theoretically calculated Archimedes and Reynolds numbers [35], the Archimedes and Reynolds numbers derived using the mean settling velocities obtained from the RTD through the statistical model, and those calculated from experimental data.

change in residence time would also be evident.

Fig. 4(d) shows the Reynolds number plotted against the Archimedes number. The plot includes a purely theoretical correlation (Turton & Clark [35]), values calculated from a statistical model based on the measured residence time distributions, and values obtained directly from experimental data. It can be seen that the theoretical correlation agrees well with both the statistical model and experimental data at lower Reynolds numbers. However, deviations become more pronounced at higher Reynolds numbers. Both the correlation and the model were calculated using average particle settling velocities, under the simplifying assumption of dry particles in pure $scCO_2$, neglecting the presence of ethanol. The observed deviations at higher Reynolds numbers are likely due to this assumption. In particular, when particle velocities increase and the dynamic viscosity of the surrounding fluid decreases, the correct estimation of the density difference ($\Delta\rho$) between the particle and fluid becomes increasingly important. Under real process conditions, the presence of ethanol alters the local fluid density and viscosity along the particle's trajectory, leading to deviations from the idealized model. Nevertheless, the theoretical correlation proves to be a useful tool for estimating average particle velocities and thus mean residence times, especially in the low Reynolds number regime, where the agreement with measured data is remarkably good.

4.2. *Influence of process parameters on residual ethanol content*

Since the successful production of aerogels in a continuous drying process depends not only on the residence time of the particles within the column but also on how effectively they are dried during this time, the residual volatile content of the aerogels was determined for all experimental runs. The results were subsequently evaluated using a statistical model. Across the investigated parameter range, the obtained aerogels consistently exhibited low residual ethanol content, with only minor variations observed. Representative TGA curves for all experimental runs are provided in the Supplementary Material (Figure S2). As a result, the statistical model applied to the residual ethanol data does not achieve the same predictive accuracy as the model developed for residence time. Nevertheless, it provides a reasonable basis for estimating the expected residual ethanol content under different sets of process parameters and thus contributes valuable insights for process optimization. Predicted versus actual plots for the residual ethanol model are shown in the Supplementary Material (Figure S1(b)), as well as the detailed ANOVA (Table S4).

Fig. 5 illustrates the residual ethanol content in the aerogels as a function of pressure (Fig. 5(a)) and residence time (Fig. 5(b)) for different drying temperatures.

In Fig. 5(a), the residual ethanol content is plotted against pressure at various temperatures. With increasing pressure, the residual ethanol content initially decreases, indicating improved drying efficiency. This is expected, since a higher pressure increases the fluid density and therefore reduces the settling velocity of the particles, which results in a longer residence time. At higher pressures, however, a slight increase in residual ethanol becomes evident. This effect arises from the interplay of two opposing mechanisms. On the one hand, increasing pressure increases the residence time and thus supports drying. On the other hand, higher pressures also reduce the diffusion coefficient of ethanol in $scCO_2$, which slows down the molecular transport from the pore network into the surrounding fluid. While residence time strongly increases at lower pressures, its increase becomes only marginal at pressures approaching 150 bar due to the asymptotic density characteristics of $scCO_2$. As a result, the positive effect of longer residence times becomes weaker, while the negative effect of reduced diffusivity becomes increasingly dominant. This combination leads to the characteristic minimum observed in all curves between 40 and 70 °C. With increasing temperature, this minimum shifts towards higher pressures. Higher temperatures enhance molecular diffusivity and partially counteract the pressure-induced reduction in diffusion, which allows efficient drying to be maintained at higher pressures. Thus, the curve at 80 °C is shifted to the right, and although a minimum is expected there as well, it lies outside the investigated pressure window. Temperatures above 80 °C were not investigated, as alginate begins to show thermal degradation around 100 °C. To ensure a safe operating margin and to avoid structural damage to the gel network, the upper temperature limit was therefore set to 80 °C. As seen in Fig. 5(a), lower residual ethanol levels are achieved at 40 °C under low-pressure conditions compared to higher temperatures. Only at elevated pressures does the temperature-induced increase in diffusion outweigh the shorter residence time, leading to improved drying. This suggests that residence time plays a dominant role at low pressure, whereas diffusion becomes more critical at high pressure. Fig. 5(b) supports this interpretation: at comparable residence times, samples dried at higher temperatures show substantially lower residual ethanol contents. This highlights that when residence time is held constant, increasing temperature leads to better drying results. Aerogels dried at 80 °C reach the lowest residual ethanol levels despite having one of the shortest residence times in the dataset.

Fig. 6 illustrates two different approaches to characterizing drying performance during continuous $scCO_2$ drying. Fig. 6(a) presents the ratio ζ, defined as the length-specific residence time τ_{res} divided by the theoretically calculated minimum drying time $\tau_{dry,min}$ using the approach of Selmer et al. [30]. This ratio was already introduced in previous works [24] and can be regarded as a measure of space–time

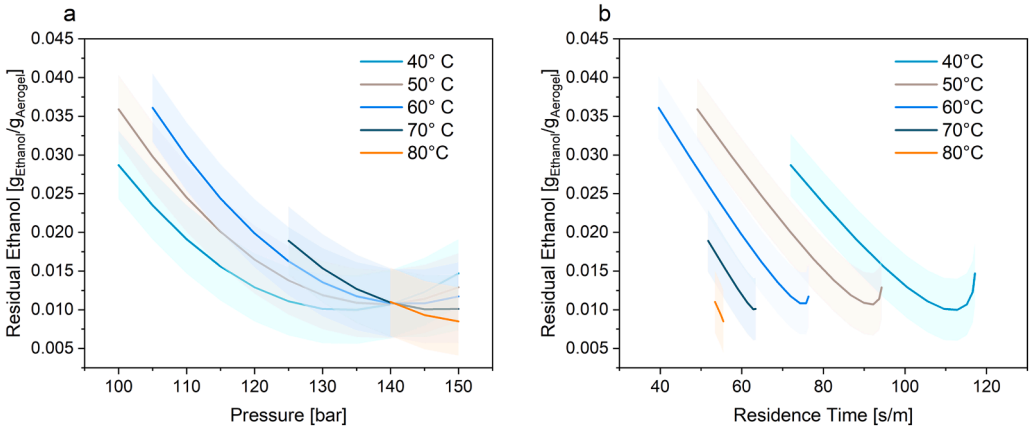

Fig. 5. Influence of process parameters on residual ethanol of dried Aerogels: a) Influence of temperature and pressure at constant CO_2 flow rate (50 g/min) and constant suspension flow rate (20 g/min) on the residual ethanol, b) Influence of temperature and specific residence time at constant CO_2 flow rate (50 g/min) and constant ethanol flow rate (20 g/min) on the residual ethanol.

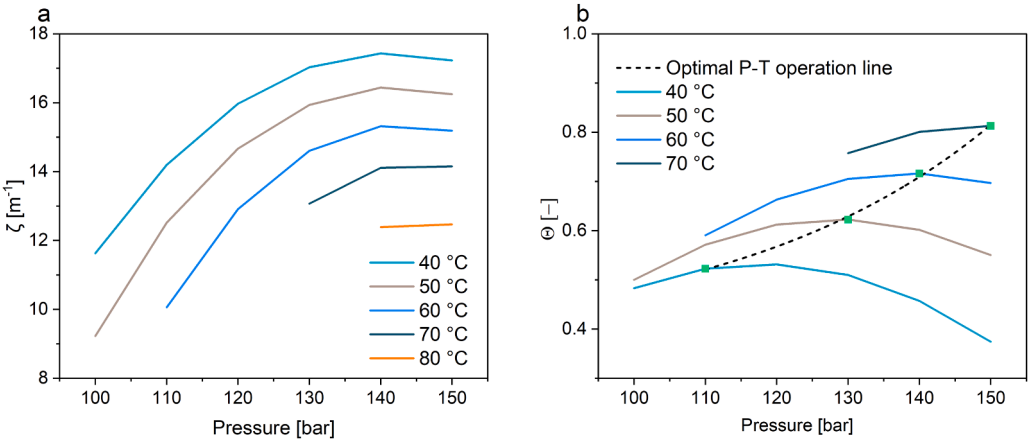

Fig. 6. Influence of operating pressure and temperature on (a) the ratio ζ between the length-specific residence time and the theoretically estimated minimum drying time, and (b) the normalized efficiency score Θ (Eq.12). All experiments were conducted at a constant CO_2 flow rate (50 g/min) and constant suspension flow rate (20 g/min).

yield. It expresses how effectively the available residence time in the column is utilized relative to the minimum theoretical drying demand. A ζ value of 1 corresponds to the ideal case in which the actual residence time exactly equals the theoretical drying time, indicating that particles remain in the column just long enough to achieve solvent removal without overdrying. Lower ζ values are thus generally associated with more favorable operation. However, since the drying times used here are purely theoretical estimates, and the actual drying times under real operating conditions are expected to be longer, ζ alone does not allow a conclusive assessment of true drying performance. This becomes evident at 100 bar and 50 °C, where ζ reaches its minimum value. While this might suggest an optimal operation regarding the space-time yield, it coincides with the highest measured residual ethanol contents in the aerogels, demonstrating that ζ alone cannot be used to assess optimal process parameters.

To better represent practical performance, an alternative metric Θ was introduced (Fig. 6(b)). Θ is defined in Eqs. (12) – (14) as the arithmetic mean of the min–max normalized and inversely scaled residence time and residual ethanol content, thereby weighting both short residence times and low residual ethanol contents equally as desirable outcomes. Unlike ζ, Θ does not quantify space–time yield, but rather indicates drying effectiveness by identifying the operating points at which both fast processing and sufficient solvent removal are achieved simultaneously. As shown in Fig. 6(b), Θ increases with rising temperature: at lower temperatures, moderate pressures yield better performance, whereas at elevated temperatures, higher pressures are required to reach optimal drying conditions. The most favorable operating point was observed at high temperatures and high pressures, where the lowest residual ethanol content was achieved in combination with a comparatively short residence time, indicating particularly effective drying.

$$\Theta = \left(\frac{\widetilde{\tau}_{res}^{-1}}{2} + \frac{\widetilde{X}_{EtOH}^{-1}}{2} \right) \tag{12}$$

$$\widetilde{\tau}_{res} = \frac{\tau_{res} - \tau_{\min}}{\tau_{\max} - \tau_{\min}} \tag{13}$$

$$\widetilde{X}_{EtOH} = \frac{X_{EtOH} - X_{\min}}{X_{\max} - X_{\min}} \tag{14}$$

The efficiency metric Θ allows the identification of an optimal pressure for each investigated temperature, representing the operating point at which drying is both most effective and achieved within the shortest residence time (green rectangle). These optima are displayed as the Θ-optimum line (black dashed curve). Connecting these individual optima across the temperature range reveals an exponential trend. From this trend, it can be deduced that the maximum Θ at 70 °C is expected to occur at around 150 bar, even though pressures beyond this value were not experimentally investigated. The progression of the optima from 40 °C to 60 °C already demonstrates that higher pressures yield no further improvement, as the density of $scCO_2$ increases only marginally at high pressures and thus no longer leads to a meaningful extension of residence time. Therefore, even if pressures above 150 bar were tested, no additional gain in Θ would be anticipated, and any marginal benefit would not justify the substantially higher energy demand associated with CO_2 compression. While Θ is of limited relevance for the studied small particles, since their residual ethanol contents were already sufficiently low to avoid any impact on the aerogel microstructure, the metric becomes significant for larger particles. In these cases, higher residual ethanol contents are expected, and identifying the optimal combination of pressure and temperature is therefore critical to ensure effective drying.

In addition to evaluating process efficiency and drying performance, the structural characteristics of the dried particles were analyzed. To assess the impact of the continuous $scCO_2$ drying on particle integrity and microstructure, key physical parameters were determined, including specific surface area, pore size distribution, and total porosity. Furthermore, particle size distributions before and after drying were measured to evaluate potential shrinkage or agglomeration effects during the continuous process. These properties provide further insight into the material quality and structural preservation achieved under the applied drying conditions.

Fig. 7 shows the particle size distributions before and after drying. The particle size distributions demonstrate that the overall morphology of the beads is largely preserved during the transformation from hydrogel to aerogel. The mean particle diameter decreased by about 15 % (from 420 μm to 358 μm), which represents a comparatively low shrinkage, and the sphericity of the aerogels was maintained at 0.89 ± 0.01. This indicates that structural collapse was minimal and the gel network almost maintained its integrity [38–40], as expected for a successful aerogel drying. This is further supported by nitrogen physisorption measurements, which reveal a mean specific surface area of 363 ± 27 m^2/g and a mean total pore volume of 3.2 ± 0.7 cm^3/g. The median pore diameter was 44.2 ± 1.6 nm, confirming mesoporosity. Full adsorption–desorption isotherms and corresponding BET fits are shown in Figure S3 of the Supplementary Material. Both values fall within literature ranges for alginate aerogels, with reported surface areas of 271–600 m^2/g and pore volumes of 3–10 cm^3/g [38,40–42]. In our case, the surface area lies around the middle of this range, whereas the pore volume is closer to the lower end. Together, these results indicate that small differences in residual ethanol content did not

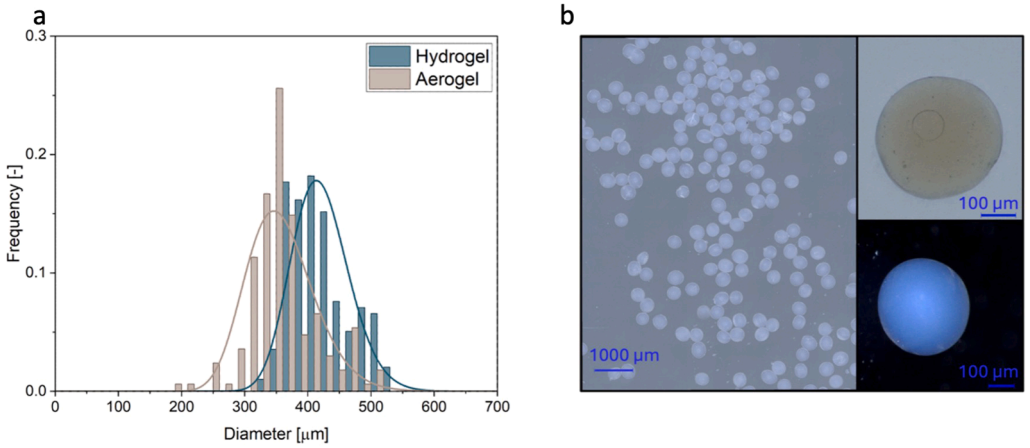

Fig. 7. (a) Particle size distribution of hydrogel beads and aerogel beads. (b) Overview of aerogel particle distribution and representative single aerogel particles.

measurably affect the microstructure and confirm that the developed continuous drying process yields structurally intact, highly porous aerogel particles.

5. Conclusions

In this study, the continuous countercurrent $scCO_2$ drying of aerogel particles was systematically analysed to understand how operating parameters influence residence time and drying performance. The experimental results also clarify how residence time and drying performance interact in a continuous countercurrent $scCO_2$ column. Residence time is primarily driven by fluid density, with strong sensitivity at low pressures and only minor increases once the density approaches its upper range within the range of parameters investigated. Drying performance is shaped by two opposing effects: longer residence times support solvent removal, while increasing pressure reduces the diffusion coefficient of ethanol in $scCO_2$. The combination of these effects explains the presence of temperature-dependent optima and why theoretical minimum-drying-time concepts underestimate real drying profiles. The newly introduced efficiency metric captures this interplay more accurately than simplified theoretical correlations.

This study provides an experimentally validated understanding of how residence time and mass transfer jointly determine drying in a continuous countercurrent $scCO_2$ column. The developed model enables targeted adjustment of residence times and residual solvent contents and is transferable to other particle sizes and materials, even though the absolute values will differ. These insights allow the identification of operating conditions that achieve reliable drying while keeping residence times and energy demands within an economically meaningful range. With this work, the second major step after the initial theoretical framework has been completed, moving the process closer to practical application. Future studies should define the operational limits of the system, including maximum particle loading, upper particle size boundaries and the minimum CO_2 flow rate required to achieve complete drying under steady-state ethanol profiles.

Author contributions

The manuscript was written through contributions of all authors. All authors have given approval to the final version of the manuscript.

Funding

The authors wish to acknowledge support for this research received from the Deutsche Forschungsgemeinschaft (DFG, German Research Foundation) for the project “Development of a continuous, scalable process for the production of aerogels” (project number 550387580).

CRediT authorship contribution statement

Irina Smirnova: Writing – review & editing, Supervision, Funding acquisition. **Baldur Schroeter:** Writing – review & editing. **Alberto Bueno:** Writing – review & editing. **Bennet Rastar:** Investigation. **Erik Manke:** Writing – review & editing, Writing – original draft, Visualization.

Declaration of Competing Interest

The authors declare that they have no known competing financial interests or personal relationships that could have appeared to influence the work reported in this paper.

Appendix A. Supporting information

Supplementary data associated with this article can be found in the online version at doi:10.1016/j.supflu.2026.106888.

Data availability

Data will be made available on request.

References

[1] N. Menshutina, P. Tsygankov, I. Khudeev, A. Lebedev, Intensification methods of supercritical drying for aerogels production, Dry. Technol. 40 (2021) 1–14, https://doi.org/10.1080/07373937.2020.1866005.
[2] C.A. García-González, M. Blanco-Vales, J. Barros, A.C. Boccia, T. Budtova, L. Durães, C. Erkey, M. Gallo, P. Herman, J. Kalmár, A. Iglesias-Mejuto, W. J. Malfait, S. Zhao, L. Manzocco, S. Plazzotta, S. Milovanovic, M. Neagu, L.E. Nita, P. Paraskevopoulou, A. Roig, R. Simón-Vázquez, I. Smirnova, Ž. Tomović, C. López-Iglesias, Review and perspectives on the sustainability of organic aerogels, ACS Sustain. Chem. Eng. 13 (2025) 6469–6492, https://doi.org/10.1021/acssuschemeng.4c09747.
[3] I.I. Khudeev, A.E. Lebedev, M.S. Mochalova, N.V. Menshutina, Modeling and techno-economic optimization of the supercritical drying of silica aerogels, Dry. Technol. 42 (2024) 812–835, https://doi.org/10.1080/07373937.2024.2318439.
[4] H. Leuenberger, New trends in the production of pharmaceutical granules: batch versus continuous processing, Eur. J. Pharm. Biopharm. 52 (2001) 289–296, https://doi.org/10.1016/S0939-6411(01)00199-0.
[5] C. Wiles, P. Watts, Continuous process technology: a tool for sustainable production, Green. Chem. 16 (2014) 55–62, https://doi.org/10.1039/C3GC41797B.
[6] A.S. Rathore, H. Agarwal, A.K. Sharma, M. Pathak, S. Muthukumar, Continuous processing for production of biopharmaceuticals, Prep. Biochem. Biotechnol. 45 (2015) 836–849, https://doi.org/10.1080/10826068.2014.985834.
[7] E.S. Langer, R.A. Rader, Continuous manufacturing: technology landscape and trends, 2013. ⟨https://www.biopharma.com/continuous.pdf⟩ (accessed May 26, 2025).
[8] K. Plumb, Continuous processing in the pharmaceutical industry: changing the mind set, Chem. Eng. Res. Des. 83 (2005) 730–738, https://doi.org/10.1205/cherd.04359.

[9] A.L. Zydney, Perspectives on integrated continuous bioprocessing — opportunities and challenges, Curr. Opin. Chem. Eng. 10 (2015) 8–13, https://doi.org/10.1016/j.coche.2015.07.005.
[10] I. Smirnova, P. Gurikov, Aerogel production: current status, research directions, and future opportunities, J. Supercrit. Fluids 134 (2018) 228–233, https://doi.org/10.1016/j.supflu.2017.12.037.
[11] F. Ruiz, J.-Y. Clavier, Method for continuous aerogel production, US11542169B2, 2023. ⟨https://patents.google.com/patent/US11542169B2/en⟩ (accessed April 20, 2023).
[12] S. Movahhed, W. Loelsberg, D. Weinrich, M. Fricke, R. Subrahmanyam, lrina, P. Smirnova, F. GurikovMissfeldt, Process for continuous supercritical drying of aerogel particles, US20220041817A1, 2022. https://patents.google.com/patent/US20220041817A1/en (accessed May 26, 2025)..
[13] E. Cuce, P.M. Cuce, C.J. Wood, S.B. Riffat, Toward aerogel based thermal superinsulation in buildings: A comprehensive review, Renew. Sustain. Energy Rev. 34 (2014) 273–299, https://doi.org/10.1016/j.rser.2014.03.017.
[14] C. Moreno-Castilla, F.J. Maldonado-Hódar, Carbon aerogels for catalysis applications: an overview, Carbon 43 (2005) 455–465, https://doi.org/10.1016/j.carbon.2004.10.022.
[15] I. Smirnova, Pharmaceutical Applications of Aerogels, in: M.A. Aegerter, N. Leventis, M.M. Koebel (Eds.), Aerogels Handb, Springer, New York, NY, 2011, pp. 695–717, https://doi.org/10.1007/978-1-4419-7589-8_31.
[16] J.P. Randall, M.A.B. Meador, S.C. Jana, Tailoring mechanical properties of aerogels for aerospace applications, ACS Appl. Mater. Interfaces 3 (2011) 613–626, https://doi.org/10.1021/am200007n.
[17] A.A. Firoozi, A.A. Firoozi, A.A. El-Abbasy, K. Aati, Enhanced perspectives on silica aerogels: novel synthesis methods and emerging engineering applications, Results Eng. 25 (2025) 103615, https://doi.org/10.1016/j.rineng.2024.103615.
[18] C.A. García-González, M.C. Camino-Rey, M. Alnaief, C. Zetzl, I. Smirnova, Supercritical drying of aerogels using CO2: Effect of extraction time on the end material textural properties, J. Supercrit. Fluids 66 (2012) 297–306, https://doi.org/10.1016/j.supflu.2012.02.026.
[19] I. Turhan Kara, B. Kiyak, N. Colak Gunes, S. Yucel, Life cycle assessment of aerogels: a critical review, J. Sol. Gel Sci. Technol. 111 (2024) 618–649, https://doi.org/10.1007/s10971-024-06455-0.
[20] I. De Marco, R. Iannone, S. Miranda, S. Riemma, An environmental study on starch aerogel for drug delivery applications: effect of plant scale-up, Int. J. Life Cycle Assess. 23 (2018) 1228–1239, https://doi.org/10.1007/s11367-017-1351-6.
[21] N.A. Sargent, W.M. Davis, Method for producing aerogels, US2868280A, 1959. ⟨https://patents.google.com/patent/US2868280A/en⟩ (accessed August 26, 2025).
[22] F. Ruiz, J.-Y. Clavier, Procede continu et installation de fabrication d'un aerogel, EP3478400B1, 2020. ⟨https://patents.google.com/patent/EP3478400B1/de?oq=EP3478400B1⟩ (accessed August 26, 2025).
[23] V. Steinhagen, A. Herber, Vorrichtung und verfahren zum kontinuierlichen hochdruckbehandeln von schüttgut sowie verwendung, WO2020127889A2 (2020). ⟨https://patents.google.com/patent/WO2020127889A2/de?oq=WO2020127889A2⟩ (accessed August 26, 2025).
[24] F. Mißfeldt, P. Gurikov, W. Lölsberg, D. Weinrich, F. Lied, M. Fricke, I. Smirnova, Continuous supercritical drying of aerogel particles: proof of concept, Ind. Eng. Chem. Res. 59 (2020) 11284–11295, https://doi.org/10.1021/acs.iecr.0c01356.
[25] P.V. Danckwerts, Continuous flow systems: distribution of residence times, Chem. Eng. Sci. 2 (1953) 1–13, https://doi.org/10.1016/0009-2509(53)80001-1.
[26] H.S. Fogler. Elements of chemical reaction engineering, Fifth edition, Prentice Hall, Boston, 2016.
[27] Y. Gao, F.J. Muzzio, M.G. Ierapetritou, A review of the Residence Time Distribution (RTD) applications in solid unit operations, Powder Technol. 228 (2012) 416–423, https://doi.org/10.1016/j.powtec.2012.05.060.
[28] A.T. Harris, J.F. Davidson, R.B. Thorpe, A novel method for measuring the residence time distribution in short time scale particulate systems, Chem. Eng. J. 89 (2002) 127–142, https://doi.org/10.1016/S1385-8947(02)00004-9.
[29] B. Schroeter, V.P. Yonkova, N.A.M. Niemeyer, I. Jung, I. Preibisch, P. Gurikov, I. Smirnova, Cellulose aerogel particles: control of particle and textural properties in jet cutting process, Cellulose 28 (2021) 223–239, https://doi.org/10.1007/s10570-020-03555-2.
[30] I. Preibisch, P. Niemeyer, Y. Yusufoglu, P. Gurikov, B. Milow, I. Smirnova, Polysaccharide-based aerogel bead production via jet cutting method, Materials 11 (2018) 1287, https://doi.org/10.3390/ma11081287.
[31] S. Pietsch, M. Schönherr, F. Kleine Jäger, S. Heinrich, Measurement of residence time distributions in a continuously operated spouted bed, Chem. Eng. Technol. 43 (2020) 804–812, https://doi.org/10.1002/ceat.201900453.
[32] P. Berne, T. Bjørnstad, P. Brisset, C. S, A. Chmielewski, G. S, G. J.M, H.A., Jin, J. S. H, Khan, M. G, M. Moreira, H. Pant, J. Thereska, Zhang, Radiotracer Residence Time Distribution Method for Industrial Applications and Environment, 2008.
[33] A. Bérard, B. Blais, G.S. Patience, Experimental methods in chemical engineering: Residence time distribution—RTD, Can. J. Chem. Eng. 98 (2020) 848–867, https://doi.org/10.1002/cjce.23711.
[34] O. Levenspiel. Chemical reaction engineering. Hauptbd, 3. ed, Wiley, New York Weinheim, 1999.
[35] R. Turton, N.N. Clark, An explicit relationship to predict spherical particle terminal velocity, Powder Technol. 53 (1987) 127–129, https://doi.org/10.1016/0032-5910(87)85007-6.
[36] A. Bueno, I. Selmer, R. S.P, P. Gurikov, W. Lölsberg, D. Weinrich, M. Fricke, I. Smirnova, First evidence of solvent spillage under subcritical conditions in aerogel production, Ind. Eng. Chem. Res. 57 (2018) 8698–8707, https://doi.org/10.1021/acs.iecr.8b00855.
[37] M.P. Dirauf, P.C. Wagner, A.S. Braeuer, Mass transfer kinetics inside bio-(aero)gels during solvent exchange and supercritical drying: on the relevance of advection, gel-porosity and a peculiarity regarding the tortuosity, J. Supercrit. Fluids 191 (2022) 105762, https://doi.org/10.1016/j.supflu.2022.105762.
[38] P. Gurikov, S.P. Raman, D. Weinrich, M. Fricke, I. Smirnova, A novel approach to alginate aerogels: carbon dioxide induced gelation, RSC Adv. 5 (2015) 7812–7818, https://doi.org/10.1039/C4RA14653K.
[39] R. Rodríguez-Dorado, C. López-Iglesias, C.A. García-González, G. Auriemma, R. P. Aquino, P. Del Gaudio, Design of aerogels, cryogels and xerogels of alginate: effect of molecular weight, gelation conditions and drying method on particles' micromeritics, Molecules 24 (2019) 1049, https://doi.org/10.3390/molecules24061049.
[40] M. Alnaief, M.A. Alzaitoun, C.A. García-González, I. Smirnova, Preparation of biodegradable nanoporous microspherical aerogel based on alginate, Carbohydr. Polym. 84 (2011) 1011–1018, https://doi.org/10.1016/j.carbpol.2010.12.060.
[41] M. Robitzer, F.D. Renzo, F. Quignard, Natural materials with high surface area. Physisorption methods for the characterization of the texture and surface of polysaccharide aerogels, Microporous Mesoporous Mater. 140 (2011) 9–16, https://doi.org/10.1016/j.micromeso.2010.10.006.
[42] B. Schroeter, I. Jung, K. Bauer, P. Gurikov, I. Smirnova, Hydrophobic modification of biopolymer aerogels by cold plasma coating, Polymers 13 (2021), https://doi.org/10.3390/polym13173000.